communications physics

A Nature Portfolio journal

Article

https://doi.org/10.1038/s42005-025-02208-9

Flat bands on a spherical surface from Landau levels to giant-quantum-number orbitals

Check for updates

Chen-Xin Jiang [1,2,3], Zi-Xiang Hu [1,2] ✉ & Bo Yang [3] ✉

Flat bands result in a divergent density of states and high sensitivity to interactions in physical systems. While such bands are well known in systems under magnetic fields, their realization and behavior in zero-field settings remain largely unexplored. Here we compare the behavior of electrons confined to a single flat band on the surface of a sphere to those in flat bands under a magnetic field. The zero-field flat band exhibits an additional $C(2)$ symmetry, which causes electrons to symmetrically cluster on opposite sides of the sphere's center when a trapping potential is introduced, resulting in a unique form of long-range "entanglement". To explore these findings experimentally, we propose a feasible setup to explore the unique properties of zero-field flat bands on spherical substrates, offering a promising route for studying interaction-driven states in spherical geometry without external fields.

The flat bands in momentum space imply divergent density of states, making the system very sensitive to interactions, often leading to many strongly correlated phenomena. Much of the research in this area is focused on periodic crystal structures, such as the fractional Chern insulators[1–3], heavy fermion systems[4–6], superconductors[7–10], Mott insulators[11,12], and so on. Research on continuous models mainly focuses on the quantum Hall effects, where topological phases emerge from electrons confined within a two-dimensional manifold subject to a strong perpendicular magnetic field. Here the flat bands, or the so-called Landau levels, are formed due to the magnetic field. In the limit of large magnetic field, only one Landau level is physically accessible at low temperature, forming a very special Hilbert space responsible for the topological physics of both the integer and fractional quantum Hall effect.

The geometries in the quantum Hall effect mainly include the disk[13], cylinder[14], sphere[15], and torus[16], among which the sphere is the only curved geometry compared to the others. The absence of boundaries on the sphere makes it particularly suitable for investigating the bulk properties of the system. Moreover, in contrast to planar geometries, the degeneracy of Landau levels in spherical geometry is finite, allowing for a clear definition of filling the Landau levels (LLs).

Even without a magnetic field, flat bands naturally arise on the surface of the sphere. The single particle kinetic energies of particles confined to the spherical surface forms gapped flat bands. Intuitively one can understand this by identifying the geometric Gaussian curvature of the sphere as analogous to a uniform "magnetic field", that nevertheless does not break time reversal symmetry. The energy quantization in this system is governed by the electron density, the radius of the sphere, and the effective mass of the electrons. Moreover, similar to Landau levels, the zero-field bands on the surface of the sphere remain strictly flat, with no dispersive bands present. The study of strongly correlated systems for electrons projected onto a specific kinetic energy flat band on the surface of a sphere in the zero field remains unexplored. Previous studies look into the Coulomb interaction model of two or three electrons on the sphere without projection into a single flat band, such as the approaches of approximate Schrödinger equations[17–19], the configuration interaction method[18,20–23]. It has been suggested that electrons can form a Wigner crystal for the strong interaction limit[19,22–25].

In this Paper, we study the physics of electrons confined to a single flat band on the surface of a conducting sphere, as well as the mixing of flat bands from strong interactions. Depending on the presence or absence of the magnetic field (i.e., magnetic monopole Q), such flat bands have distinct physical characteristics with or without strong interaction. Starting from a single electron, we find that the flat band with $Q = 0$ possesses an additional $C(2)$ symmetry. This leads to the curious phenomenon that within a single flat band, electrons cannot be localized in real space with local confining potentials. We can thus easily create a pair of "Bell state" localized simultaneously at the North Pole and South Pole of the sphere with long-range entanglement. Subsequently, we study the impact of the trapping potential on the rotational symmetry of the system. While a discrete array of trapping potentials always break the rotational invariance on the surface of the sphere, it is not necessarily the case within a single flat band. Moreover, due to the $C(2)$ symmetry of the flat band $Q = 0$, fewer trapping potentials are

[1]Department of Physics, Chongqing University, Chongqing, 401331, People's Republic of China. [2]Chongqing Key Laboratory for Strongly Coupled Physics, Chongqing University, Chongqing, 401331, People's Republic of China. [3]Division of Physics and Applied Physics, Nanyang Technological University, Singapore, 637371, Singapore. ✉e-mail: zxhu@cqu.edu.cn; yang.bo@ntu.edu.sg

needed to maintain the $\hat{L}_z$ rotational symmetry of the system, as compared to the flat bands with $Q > 0$. We also analyze the two-body interaction within these flat bands, and discovered that the effective interaction in $Q = 0$ bands are very long-range compared to those in $Q > 0$, even from a very short-range bare interaction in the real space. This leads to much stronger band mixing effects in the absence of the magnetic field.

Results

Single particle flat bands

The single-electron Hamiltonian on spherical surface with a magnetic monopole of strength Q at the center of the sphere is[15]

$$\hat{H}_k = \frac{\mathbf{L}^2 - \hbar^2 Q^2}{2m_e R^2}, \tag{1}$$

where $\mathbf{L}$ is orbital angular momentum, $\hbar$ is the reduced Planck constant, m_e is the effective mass of an electron and R is the radius of the sphere. We can easily get the Hamiltonian's eigenvalues $E_k^l = \frac{l(l+1)\hbar^2 - \hbar^2 Q^2}{2m_e R^2}$, and the eigenstates are given by the monopole harmonics $Y_{Q,l,m}$[26,27], satisfying $\mathbf{L}^2 Y_{Q,l,m} = l(l+1)\hbar^2 Y_{Q,l,m}$ and $\hat{L}_z Y_{Q,l,m}(\mathbf{\Omega}) = m\hbar Y_{Q,l,m}(\mathbf{\Omega})$, where l and m denote orbital angular momentum $\mathbf{L}$ and its z component $\hat{L}_z$ respectively, and $\mathbf{\Omega}$ is the angular coordinates θ and ϕ on the sphere. For the case of $Q > 0$, we choose the latitudinal gauge

$$\mathbf{A} = -\frac{\hbar Q}{eR}\cot\theta \hat{e}_\phi, \tag{2}$$

and the monopole harmonics Y_{Qlm} can be expressed using Wigner's d-function $d_{m,Q}^{(l)}(\theta)$[27]. Its explicit form is given by

$$Y_{Q,l,m}(\mathbf{\Omega}) = \sqrt{\frac{2l+1}{4\pi}} e^{i(m+Q)\phi} d_{m,Q}^{(l)}(\theta). \tag{3}$$

The kinetic energy levels exhibit a series of flat bands with degeneracy $2l + 1$. For the Hamiltonian of zero field $Q = 0$, its eigenstates are also called spherical harmonic functions $Y_{0,l,m} = Y_{l,m}$

$$Y_{l,m}(\mathbf{\Omega}) = \sqrt{\frac{2l+1}{4\pi}}\sqrt{\frac{(l-m)!}{(l+m)!}} P_l^m[\cos(\theta)] e^{im\phi}, \tag{4}$$

where $P_l^m(x)$ is associated Legendre polynomial.

We focus on the dynamics within the topmost unfilled lth flat band where l is fixed and large, assuming that all orbitals with angular momentum less than l are filled with electrons. Consequently, as the particle density approaches infinity, we can have a "flat band" with an infinite number of degenerate states as well as an infinitely large energy gap. This is analogous to the Landau levels in the limit of the large system sizes (the thermodynamic limit), where the energy gap is non-vanishing with an infinite number of degenerate states in a single Landau level. If we fix l (thus the degeneracy within the flat band), the Landau level index is given by $l - Q$ with $Q = l$ being the Lowest Landau level (LLL). It is well known that the eigenstates are Gaussian localized (see Fig. 1a). The very special $Q = 0$ is the case of zero magnetic field. From some perspectives this is the infinite Landau level limit ($l/Q \to \infty$), though the qualitative difference is the presence of the time reversal symmetry, so the spherical harmonics possess $C(2)$ symmetry (see Fig. 1b). In addition, from Eq. (1), it can be concluded that the gap ΔE_k^l between the flat band with orbital angular momentum l and the flat band with orbital angular momentum $l + 1$ is $\frac{(l+1)\hbar^2}{m_e R^2}$. Unlike the equidistant distribution of Landau levels in a plane, the gap between adjacent flat bands on the sphere gradually increase as l increases. While Landau levels on the sphere have been extensively studied, with the total flux through the surface of the sphere is an integer $2Q$ times the unit magnetic flux, leading to $2Q + 2n + 1$ states in the nth Landau level (nLL), in this work we will study

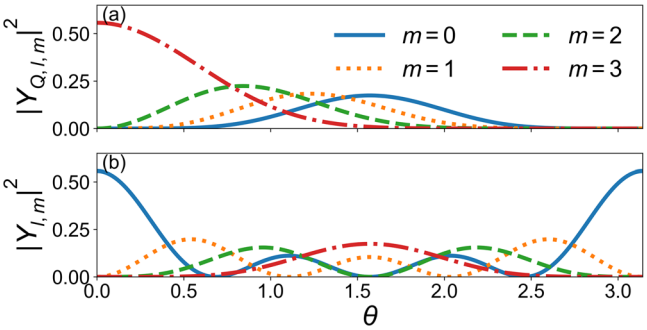

Fig. 1 | Single-particle density distributions within a flat band. a The square modulus of the monopole harmonics $Y_{Q,Q,m}$ with the strength of the magnetic monopole $Q = 3$ and $\phi = 0$ in the lowest Landau level, where m is z component of the orbital angular momentum, θ and ϕ are the angular coordinates. Blue solid, orange dotted, green dashed and red dash-dotted lines correspond to $m = 0$, 1, 2 and 3, respectively. **b** The square modulus of the spherical harmonic functions $Y_{l,m}$ with orbital angular momentum $l = 3$ and $\phi = 0$. Source data are provided in the Supplementary Data.

the flat band at $Q = 0$, so the orbital angular momentum l must be restricted to integer values.

Localization in flat bands

For temperature lower than the band gap, the physical Hilbert space is a single flat band with degeneracy $2l + 1$. Such flat bands are already special when we look at how we can localize a single particle within this flat band in real space. We introduce a 1-body delta trapping potential $V^\delta(\mathbf{\Omega})$, where $\mathbf{\Omega}$ is the position of the electron. We can use the Legendre expansion and the addition theorem of spherical harmonics to calculate the matrix elements of the one-body potential

$$\begin{aligned}\mathbf{V}^{\delta,Q}_{l_1,m_1,l_2,m_2} &= \langle Q, l_1, m_1 | V^\delta(\mathbf{\Omega}) | Q, l_2, m_2\rangle \\ &= \sum_{l'=|l_1-l_2|}^{l_1+l_2} U_{l'}^\delta \sqrt{\frac{4\pi(2l_1+1)(2l_2+1)}{2l'+1}} \\ &\quad \cdot (-1)^{Q+m_1+l'+l_1+l_2} Y^*_{l',m_1-m_2}(\mathbf{\Omega}_0) \\ &\quad \cdot \begin{pmatrix} l_1 & l' & l_2 \\ -Q & 0 & Q \end{pmatrix}\begin{pmatrix} l_2 & l' & l_1 \\ m_2 & m_1-m_2 & -m_1 \end{pmatrix},\end{aligned} \tag{5}$$

where $|Q, l, m\rangle$ denotes $Y_{Q,l,m}$, $\mathbf{\Omega}_0$ is the position of the delta trapping potential in the real space on the surface of the sphere, and the last two parentheses are wigner-3j symbols, which can be calculated by Clebsch-Gordan coefficient[28]. Furthermore, we just consider the lth level, so $l_1 = l_2 = l$. $U_{l'}^\delta$ satisfies $V^\delta(\mathbf{\Omega}) = \sum_{l'=0}^\infty P_{l'}(\cos\theta) U_{l'}^\delta$, where

$$U_{l'}^\delta = \frac{2l'+1}{2}\int_{-1}^{1} V^\delta(\mathbf{\Omega}) P_{l'}(\cos\theta) d\cos\theta, \tag{6}$$

where $P_l(x)$ is the Legendre polynomial, and θ is the angle between the position of the electron and the position of the potential. For delta potential

$$V^\delta(\mathbf{\Omega}) = W_\delta \delta^{(2)}(|\mathbf{\Omega} - \mathbf{\Omega}_0|), \quad U_{l'}^\delta = W_\delta \frac{2l'+1}{4\pi}, \tag{7}$$

where W_δ is the strength of the delta potential. To account for the effects of band mixing, the system's Hamiltonian can be expressed as

$$\hat{H}_{\text{trap}} = \hat{H}_k + \sum_{l_1,l_2,m_1,m_2} \mathbf{V}^{\delta,Q}_{l_1,m_1,l_2,m_2} C_{m_1}^{l_1\dagger} C_{m_2}^{l_2}, \tag{8}$$

where $C_m^{l\dagger}$ and C_m^l denote the creation and annihilation operators for the lth kinetic energy level, respectively. By diagonalizing the Hamiltonian $\hat{H}_{\text{trap}}$,

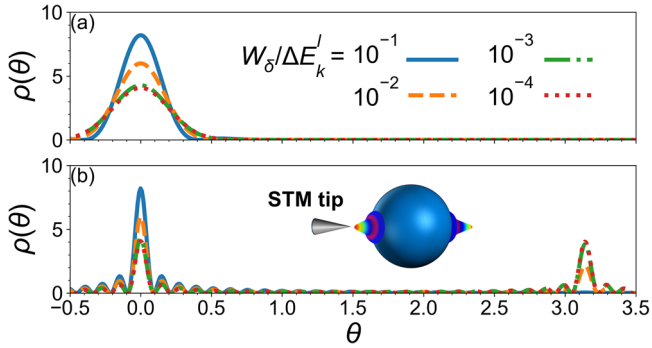

Fig. 2 | Excited-state density under a delta potential. The density profile ρ of the excited state of a delta potential located at the North Pole for the lth and $(l+1)$th flat bands mixing with orbital angular momentum $l = 25$. **a** The strength of the magnetic monopole $Q = l$ and $\phi = 0$, where θ and ϕ are the angular coordinates. Blue solid, orange dotted, green dashed and red dash-dotted lines represent $W_\delta/\Delta E_k^l = 10^{-1}, 10^{-2}, 10^{-3}$ and 10^{-4}, where W_δ is the strength of the delta potential and ΔE_k^l is the flat-band gap. **b** $Q = 0$ and $\phi = 0$. The gray cone marks a scanning tunneling microscopy (STM) tip applying a delta potential at one end of the blue sphere, resulting in simultaneous electron density accumulation at both ends. Source data are provided in the Supplementary Data.

we investigate the localization behavior of the electron within a single band and under strong band mixing conditions.

In the lowest Landau level, it is known that with a local impurity potential (e.g., in the form of a delta trapping potential), electrons can be Gaussian localized in the real space as a coherent state as shown in Fig. 2a. As the index of Landau level increases, the density distribution oscillations of the excited state become more and more pronounced, and the general expression of the real space wavefunction of the localized state at the origin $\mathbf{\Omega}_0 = (0, 0)$ in the nth Landau level can be written as

$$\psi(\mathbf{\Omega}) = \sum_{m=-Q-n}^{Q+n} Y^*_{Q,Q+n,m}(\mathbf{\Omega}_0) Y_{Q,Q+n,m}(\mathbf{\Omega}). \tag{9}$$

Thus as Q decreases, it is increasingly difficult to localize a single electron within a flat band, if the impurity potential is smaller than the band gap.

In the case of zero field with $Q = 0$, Fig. 2b shows that the delta trapping potential produces a qualitatively different effect. Electrons tend to cluster simultaneously at positions that are diagonally opposite on the surface of the sphere. That is to say, within a single flat band, if we apply a delta potential at the North Pole, we will similarly observe electron clustering at the South Pole.

When the delta potential is strong enough to mix a few flat bands, electrons become more localized and concentrate at a single point regardless of the presence of a magnetic field, as shown in Fig. 2. It indicates that in the case of a zero magnetic field, band mixing breaks the $C(2)$ symmetry of the system. This is reasonable; for instance, if a delta potential with infinitely strong negative strength is introduced at the North Pole, the electron becomes fully localized at a single point, which corresponds to the limit of large band mixing. This is why it is difficult to observe this special phenomenon at $Q = 0$ in reality, as it requires the strength of the impurity potential to be much smaller than the gap ΔE_k^l, as shown in Fig. 2.

Rotational symmetry in flat bands

The special properties of the flat band Hilbert space are also reflected in its robustness of spatial symmetry. In general with localized one-body potentials or disorder, all rotational symmetries are broken. However, in a single flat band, this issue is more subtle. Within the flat band, the single particle $\mathbf{L}^2$ is always a good quantum number. This is because the influence of disorder is significantly smaller than the bandwidth, allowing the system to be regarded as a single band and preventing the mixing of different flat bands. Consequently, the only quantum number that can be affected by the disorder is $\hat{L}_z$. A single delta potential does not affect $\hat{L}_z$; when we introduce two such potentials, we need to place them diagonally on the sphere to ensure that $\hat{L}_z$ is still a good quantum number. When the number of these potentials increases the rotational symmetry is generally broken, however it can be restored if the number of delta potentials is large enough and uniformly distributed, due to the unique properties of a single flat band.

For simplicity, we introduce delta potentials at equidistant points along the equator, and ask if rotational symmetry about the z-axis is broken, or if $\hat{L}_z$ still gives a good quantum number. Naively this would not be the case for any number of delta potential in the full Hilbert space, however within a single flat band the situation is more subtle. For $Q > 0$, when the number of delta potentials, N_δ, satisfies $N_\delta \geq 2l + 1$, $\hat{L}_z$ becomes a good quantum number. In contrast, for $Q = 0$, we find that $\hat{L}_z$ remains a good quantum number even when $N_\delta < 2l + 1$, provided that N_δ is odd and greater than the orbital angular momentum l. The rigorous proofs for the above phenomenon are presented in Supplementary Note 1 and 2.

This observation can also be understood intuitively as follows. Within the flat band with angular momentum l, there are $2l + 1$ states, and this implies that only discrete symmetry of $C(2l)$ is present. Consequently, if the Hamiltonian also has the same discrete symmetry, $\hat{L}_z$ is restored as a good quantum number. For the flat band with zero field, the situation is slightly different due to the additional inversion symmetry of the system. When the number of delta potentials is odd, it effectively corresponds to doubling the number of delta potentials in the system. As a result, compared to systems with $Q > 0$, the zero-field system requires fewer delta potentials to restore rotational symmetry $\hat{L}_z$. In the full Hilbert space, however, $\hat{L}_z$ becomes a good quantum number only in the limit where the number of delta potentials along the equator approaches infinity.

When more than one electron is present, the total angular momentum $\mathbf{L}^2 = \sum_{ij} \mathbf{L}_i \mathbf{L}_j$ is generally no longer a good quantum number in the presence of impurities. However, due to the peculiarity of the Hilbert space of a single flat band, the breaking of rotational symmetry is suppressed if we add delta potentials as evenly distributed as possible on the sphere. We investigate the uniformity of the potential distributions within the system by analyzing the bandwidth Δ_b of the delta potential spectrum. Here, Δ_b is defined as the difference between the maximum and minimum energy of the spectrum. When the bandwidth is sufficiently narrow, this can be interpreted as delta potentials being isotropically distributed over the surface of a sphere. While it is relatively straightforward to achieve a uniform distribution of delta potentials in toroidal geometries[29], accomplishing this on a spherical surface presents significant challenges that have been extensively addressed in the literature[30–33], and a good solution is the Fibonacci lattice[33], as shown in Fig. 3, where the coordinates of the ith point (x_i, y_i, z_i) on a unit sphere are as follows

$$\begin{aligned} z_i &= \frac{2i-1}{N_\delta - 1}, \\ x_i &= \sqrt{1 - z_i^2}\cos(2\pi i\eta), \\ y_i &= \sqrt{1 - z_i^2}\sin(2\pi i\eta), \end{aligned} \tag{10}$$

where $\eta = \frac{\sqrt{5}-1}{2}$ is the golden ratio.

As shown in Fig. 3, We find that when $N_\delta > 2Q$, the energy bandwidth Δ_b decreases rapidly in the lowest Landau level. This suggests that even in the presence of Fibonacci lattice delta potentials, which break rotational invariance in the Hilbert space, the rotational symmetry is still well approximated. This finding aligns with similar studies conducted on torus and disk geometries[34], showing that rotational invariance is very robust against a superlattice with lattice constant smaller than the magnetic length that does not mix different LLs. Similar to the case on the torus, the bandwidth is maximum when the number of delta potentials is equal to the number of magnetic fluxes, at which the rotational invariance is broken the most.

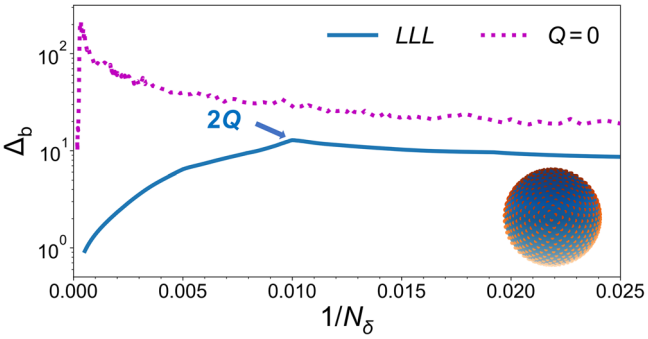

Fig. 3 | Bandwidth variation and Fibonacci lattice on the sphere. Energy-bandwidth as a function of $1/N_\delta$ and the number of orbitals $N_O = 101$, where the peak of the line representing the lowest Landau level (LLL) corresponds to $N_\delta = 2Q = 100$. N_δ is the number of delta potentials and Q is the strength of the magnetic monopole. The blue solid line represents the LLL, while the purple dash-dotted line denotes the flat band with $Q = 0$. The orange dots indicate a schematic Fibonacci lattice arranged on the surface of the blue sphere. Source data are provided in the Supplementary Data.

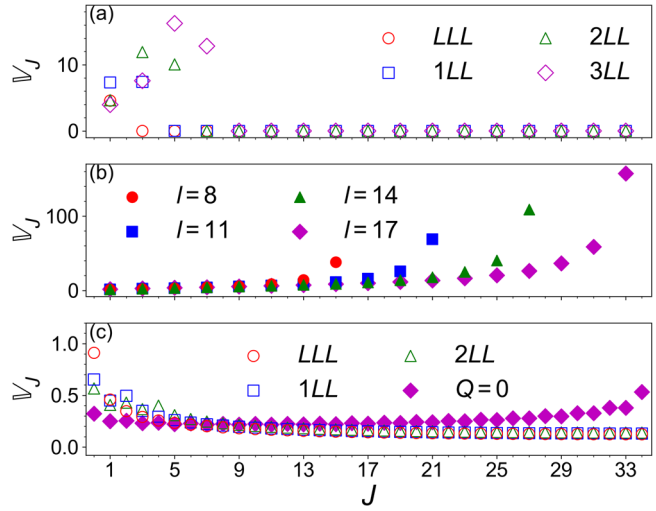

Fig. 4 | Pseudopotential parameters of the Trugman-Kivelson interaction. Q is the strength of the magnetic monopole. Since for the $Q = 0$ flat band, the system no longer has a magnetic length, making the sphere's radius the only relevant length scale, we perform an energy normalization by taking the radius of the sphere with zero field to be equal to that of the lowest Landau level. **a** Pseudopotential parameters of the Trugman-Kivelson interaction in different Landau level with orbital angular momentum $l = 17$. Red open circles (LLL), blue open squares (1LL), green open triangles (2LL), and purple open diamonds (3LL) represent the lowest, first, second, and third Landau levels, respectively. **b** Pseudopotential parameters of the Trugman-Kivelson interaction in the lth flat band with $Q = 0$. Red filled circles, blue filled squares, green filled triangles, and purple filled diamonds represent $l = 8$, 11, 14 and 17, respectively. **c** Pseudopotential parameters of the Coulomb interaction in different flat band with $l = 17$. Source data are provided in the Supplementary Data.

In contrast, for the case of $Q = 0$, the magnetic length no longer serves as the fundamental length scale, although the number of states within a single flat band remains finite in analogy to the Landau levels. Consequently, the bandwidth Δ_b is significantly larger than in the case of $Q > 0$, even when N_δ exceeds the number of states in a single flat band. As N_δ becomes very large, however, Δ_b rapidly decreases. Nevertheless, for the same system size and the same value of N_δ, the rotational invariance of the $Q > 0$ band is consistently more robust, as evidenced by its smaller bandwidth Δ_b.

Interaction within flat bands

We now move on to discuss the differences between the flat band with zero field and the Landau levels from the perspective of interactions. We first look at the regime when the interaction energy scale is small compared to the band gap, so that we can ignore the band mixing effect. The interaction Hamiltonian projected onto the kinetic energy level l in the spherical geometry, can be solved by projecting it into the center of mass space[15], and the matrix elements of the Hamiltonian can be written as

$$\begin{aligned}\hat{H}^l_{\text{int}} = &\sum_{m_1,m_2}\sum_{m_3,m_4}\sum_{J,M}\sum_{J',M'}\langle Q,l,m_1,l,m_2|Q,l,l,\mathbb{J},M\rangle \\ &\cdot\langle Q,l,l,\mathbb{J},M|U(\mathbf{\Omega}_1-\mathbf{\Omega}_2)|Q,l,l,\mathbb{J}',M'\rangle \\ &\cdot\langle Q,l,l,\mathbb{J}',M'|Q,l,m_3,l,m_4\rangle C^\dagger_{m_1}C^\dagger_{m_2}C_{m_4}C_{m_3},\end{aligned} \tag{11}$$

where $U(\mathbf{\Omega}_1 - \mathbf{\Omega}_2)$ is the interaction of two electrons, $\mathbb{J}$ and M denote coupled total angular momentum and its z component, and $Q = 0$ denotes zero field. $\langle l, m_1, l, m_2|l, l, \mathbb{J}, M\rangle$ is Clebsch-Gordan coefficient[28], and $\langle l, l, \mathbb{J}, M|U(\mathbf{\Omega}_1 - \mathbf{\Omega}_2)|l, l, \mathbb{J}', M'\rangle = \mathbb{V}_{\mathbb{J}}\delta_{J,J'}\delta_{M,M'}$ is the 2-body pseudopotential parameter, which reflects the interaction between two electrons, and $J = 2l - \mathbb{J}$ is the relative angular momentum.

We start with the short-range Trugman-Kivelson (TK) type interaction[35]. For a fermionic system, it can be written as

$$U^\delta(\mathbf{\Omega}_1 - \mathbf{\Omega}_2) = \nabla^2\delta(|\mathbf{\Omega}_1 - \mathbf{\Omega}_2|), \tag{12}$$

and the corresponding pseudopotential parameters are shown in Fig. 4. For the lowest Landau level, it is well known that the 2-body pseudopotential corresponding to the TK interaction is $\mathbb{V}_1$. This is no longer the case in higher LLs: we find that with the same contact interaction in real space, the corresponding pseudopotential is $\mathbb{V}_1 + \mathbb{V}_3 + \cdots + \mathbb{V}_{2l-1}$ in the lth Landau level. Thus, even though different LLs are topologically equivalent, there are still qualitative differences. For example, the exact Laughlin state at $\nu = 1/3$ can only be realized in the LLL. In higher LLs the interaction tends to become more long ranged in the pseudopotential basis. This is also fundamentally related to the increase of the trace of the Fubini-Study metric in higher LLs[36].

As we can understand the $Q = 0$ case as the limit of an infinite number of LLs, it is not surprising that even with a very short-range interaction in the real space, the effective interactions are very long-range in the pseudopotential basis compared to when there is a magnetic monopole, as shown in Fig. 4(b). This significant difference prevents the realization of a uniform ground state within the partially filled flat band with realistic Coulomb interactions, in contrast to the case of $Q > 0$, as shown in Supplementary Note 3.

Strong interaction limit and flat band mixing

So far we only focused on the cases where the gap between the flat bands is infinite with no band mixing especially from the electron-electron interaction. In experiments the band gap is always finite, and the interaction energy scale is not necessarily small compared to the band gap. The resulting band mixing from interaction can significantly affect the dynamics of electrons. For example in the fractional quantum Hall effect, Landau levels mixing (LLM) breaks the particle-hole symmetry of the two-body interaction system and leads to the emergence of many non-Abelian states[37–39]. When the Coulomb interaction is smaller than the energy gap between the flat bands, we can treat the interaction as a perturbation to solve for an effective single Landau level model[40–43]. However, in many experimental samples, the strength of interaction is often close to or greater than the gap of flat bands[44,45], rendering the perturbation theory ineffective. Therefore, we choose a nonperturbative approach by directly mixing two flat bands. Previous studies have shown that excluding higher Landau levels will not have a significant impact on the results[42], and the valence states are polarized[46,47], with excitations of different spin not substantially affecting the crucial physics of the system[47]. These viewpoints can support the validity of our model. In order to compare the different properties of the system with zero field, we mix the two flat bands with zero field and do not consider the electron spin.

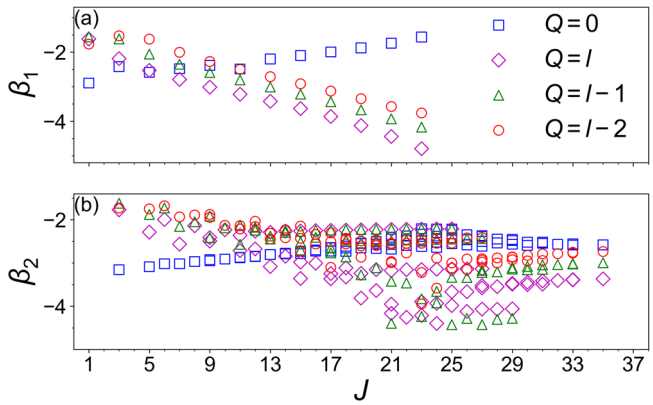

Fig. 5 | Modifications to two-body and three-body pseudopotentials. The effective pseudopotential parameters for the lth and $(l+1)$th flat bands mixing with orbital angular momentum $l = 12$ and different strength of magnetic monopole Q, where the sphere radius for $Q = 0$ is the same as that for $Q = l$. All modifications are negative values. **a** $\beta_1 = \lg\left|\frac{\mathbb{V}_J^{2-\mathrm{bodym}} - \mathbb{V}_J^{2-\mathrm{body}}}{\mathbb{V}_J^{2-\mathrm{body}}}\right|$ represents the logarithmic ratio of the modification to the two-body pseudopotential parameters, to the two-body pseudopotential parameters within a single flat band. Blue open squares, purple open diamonds, green open triangles, and Red open circles represent $Q = 0, l, l-1$, and $l-2$, respectively. **b** $\beta_2 = \lg\left|\frac{\mathbb{V}_{J,\alpha}^{3-\mathrm{bodym}}}{\mathbb{E}_{J,\alpha}}\right|$ denotes the logarithmic ratio of the modification to the three-body pseudopotential parameters, to the three-electron energy $\mathbb{E}_{J,\alpha}$ from the two-body effective interaction $\sum_J \mathbb{V}_J^{2-\mathrm{bodym}} \hat{\mathbb{H}}_J^{2-\mathrm{bodym}}$. Source data are provided in the Supplementary Data.

The Hamiltonian of the system with flat band mixing (FBM) can be written as

$$\begin{aligned}\hat{H}_{\mathrm{FBM}} =& \hat{H}_k + \hat{H}_{\mathrm{coulomb}},\\ \hat{H}_k =& \sum_i \frac{\mathbf{L}_i^2 - \hbar^2 Q^2}{2m_e R^2},\\ \hat{H}_{\mathrm{coulomb}} =& \frac{e^2}{4\pi\epsilon R}\sum_{m_1,m_2}\sum_{m_3,m_4}\sum_{l_1,l_2}\sum_{l_3,l_4}\langle Q, l_1, m_1, l_2, m_2|\\ &\cdot\frac{1}{|\mathbf{\Omega}_1 - \mathbf{\Omega}_2|}|Q, l_3, m_3, l_4, m_4\rangle C_{m_1}^{l_1\dagger} C_{m_2}^{l_2\dagger} C_{m_4}^{l_4} C_{m_3}^{l_3},\end{aligned} \tag{13}$$

where ϵ is the permittivity. Due to the ratio of the Coulomb interaction to the gap of flat bands $\hat{H}_{\mathrm{coulomb}}/\Delta E_k^l \to R$, we can actually control the relative strength of the Coulomb interaction by changing the radius of the sphere.

The effective Hamiltonian of the projected interaction can be written as

$$\hat{H}_{\mathrm{eff}} = \sum_J \mathbb{V}_J^{2-\mathrm{body}} \hat{\mathbb{H}}_J^{2-\mathrm{body}}, \tag{14}$$

which corresponds to the two-body pseudopotential parameter $\mathbb{V}_J^{2-\mathrm{body}}$ described in Eq. (11), and $\hat{\mathbb{H}}_J^{2-\mathrm{body}}$ is the two-body pseudopotential interaction with total relative angular momentum J without FBM. In general, the effective Hamiltonian within a single flat band that captures the band mixing effect is given by two-body or more pseudopotentials as shown below:

$$\hat{H}_{\mathrm{effm}} = \sum_{i=2}\sum_{J,\alpha} \mathbb{V}_{J,\alpha}^{i-\mathrm{bodym}} \hat{\mathbb{H}}_{J,\alpha}^{i-\mathrm{bodym}}, \tag{15}$$

where $\hat{\mathbb{H}}_{J,\alpha}^{i-\mathrm{bodym}}$ is the i-body pseudopotential interaction with total relative angular momentum J within a single band[48], $\mathbb{V}_{J,\alpha}^{i-\mathrm{bodym}}$ denotes the corresponding pseudopotential parameters, and α denotes the degeneracy of such pseudopotentials with the same total relative angular momentum. The energy spectrum of Eq. (15) is defined to match the low-energy part of the full Hamiltonian in Eq. (13) for any number of electrons. Consequently, the modification to the two-body pseudopotential parameter due to FBM can be easily determined as $\mathbb{V}_J^{2-\mathrm{bodym}} - \mathbb{V}_J^{2-\mathrm{body}}$. Similarly, the modification to the three-body pseudopotential parameter is given by $\mathbb{V}_{J,\alpha}^{3-\mathrm{bodym}}$, which can be determined by subtracting the three-electron energy contribution of the two-body effective interactions, $\sum_J \mathbb{V}_J^{2-\mathrm{bodym}} \hat{\mathbb{H}}_J^{2-\mathrm{bodym}}$, from the low-energy part of the Hamiltonian in Eq. (13) for three electrons. Unlike the two-body pseudopotential coefficients, the allowed values of J for the three-body pseudopotential coefficients follow the relation $J = 3n_1 + 2n_2$ with $n_1 \geq 1$, $n_2 \geq 0$, $n_1, n_2 \in \mathbb{Z}$[48], indicating that for a given J, multiple pseudopotential coefficients may exist.

The mixing of the lth and $(l+1)$th flat bands results in the pseudopotential modifications for the two-body and three-body interactions in the lth band, as shown in Fig. 5. As Q decreases, the modifications of band mixing on the large-J components of the pseudopotential parameters become increasingly significant, In particular, at $Q = 0$, the modifications to the large-J components are the strongest and constitute the primary contribution.

Discussion

In summary, the flat band with $Q = 0$ exhibits a range of intriguing properties, one of which is its ability to host long-range entangled states with a simple experimental setup. Specifically, as discussed in the Results section titled Localization in flat bands, a single flat band offers a rather natural setting for long-range "entanglement", especially if the sphere is sufficiently large. A conducting spherical shell can thus be used as a convenient platform for hosting a "Bell pair", when a pair of electrons with opposite spins is added to the shell in the presence of a localization potential at the North Pole (e.g., from a scanning tunneling microscopy tip). Due to the special $C(2)$ symmetry of the system with $Q = 0$, the probability density of the electrons is concentrated at opposite ends of the sphere even though the two ends are spatially well separated, and the local potential is only applied at one end. The single particle long-range entanglement of the electrons of opposite spin (e.g., if they form a singlet) implies a spin-up measured at the North Pole forces a spin-down to be measured at the South Pole, or vice versa, as shown in Fig. 6a.

Several conditions need to be satisfied in the experiments for the zero-field (i.e., $Q = 0$) flat band to be realized with large enough band gap as compared to temperature or disorder in the system. Explicitly the radius R of the sphere must satisfy $R \ll \sqrt{\frac{(l+1)\hbar^2}{k_B T m_e}}$, where k_B is the Boltzmann constant. Hence, if we take $\Delta E_k^l \geq 10 k_B T$, this gives the maximum value of radius

$$R_{\max} = \sqrt{\frac{(l+1)\hbar^2}{10 k_B T m_e}}. \tag{16}$$

Furthermore, for the flat band with orbital angular momentum l, lower flat bands are completely filled, requiring a total number of $2l^2$ electrons. The relationship between the electron density ρ_e and the radius of the sphere is thus

$$R = \sqrt{\frac{l^2}{2\pi\rho_e}}. \tag{17}$$

To determine the crossover temperature T_c, we use the condition $R = R_{\max}$, and

$$T_c = \frac{(l+1)\pi\hbar^2\rho_e}{5 l^2 k_B m_e}. \tag{18}$$

Realizing the flat bands at higher temperatures and on larger spherical surfaces requires materials with a sufficiently small effective mass and a high electron density, as shown in Fig. 6(b) and (c). If a larger spherical surface is

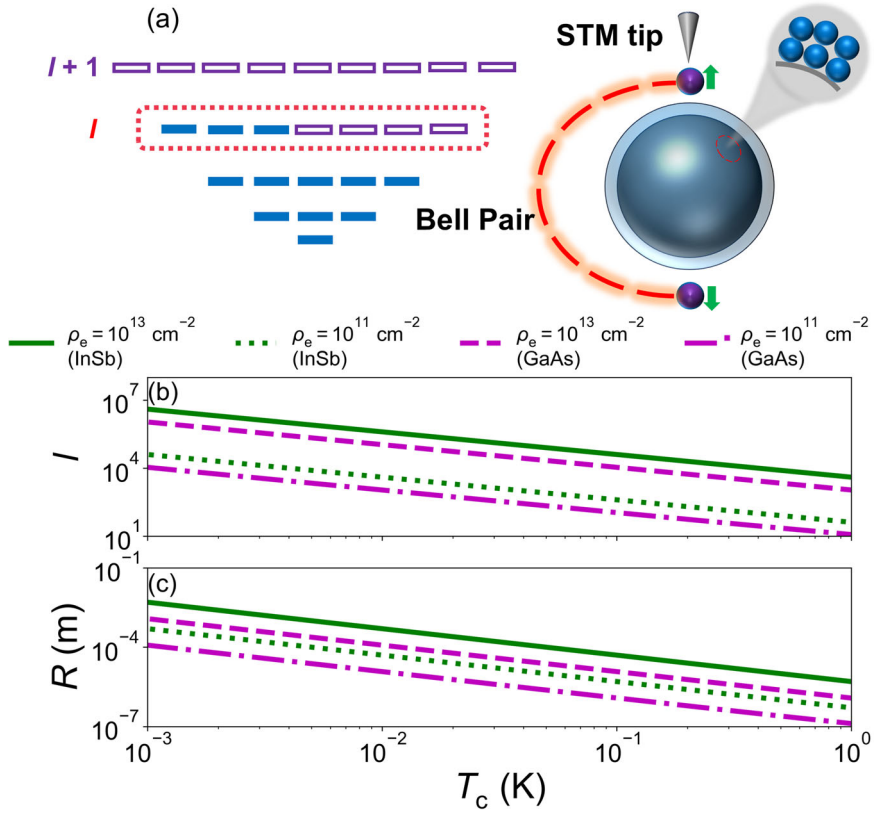

Fig. 6 | Experimental concept and physical parameters for realizing spherical flat bands. a The figure schematically illustrates the flat band on the spherical surface with the strength of the magnetic monopole $Q = 0$ and a zero-field system designed to host a Bell pair, where the blue solid rectangles represent orbitals occupied by electrons, the purple hollow rectangles indicate unoccupied orbitals, and the region enclosed by red dotted lines corresponds to the partially filled flat band with orbital angular momentum l. The inner sphere represents the spherical substrate, while the outer shell represents a layer of two-dimensional electron gas (2DEG), such as that in indium antimonide (InSb) and gallium arsenide (GaAs). The gray cone indicates the scanning tunneling microscopy (STM) tip applying a localized potential. The purple spheres at the North Pole and South Pole denote a pair of entangled electrons, with green arrows indicating the spin orientations of each electron. **b** The orbital angular momentum l as functions of crossover temperature T_c for different electron densities ρ_e. Green solid and dotted lines correspond to InSb with $\rho_e = 10^{13}\text{cm}^{-2}$ and 10^{11}cm^{-2}, respectively; purple dashed and dash-dotted lines correspond to GaAs with the same electron densities. **c** The radius R as functions of crossover temperature T_c for different ρ_e. Source data are provided in the Supplementary Data.

required, the experimental temperature must be reduced. Alternatively, increasing the electron density provides another feasible approach. Experimentally, several methods have been developed to achieve higher electron densities[49]. We can look at two common materials indium antimonide (InSb) and gallium arsenide (GaAs), with effective masses 0.014 m_0 and 0.067 m_0, where m_0 is the free electron mass, and electron densities $2.4 \times 10^{11}\text{cm}^{-2}$ and $1.3 \times 10^{11}\text{cm}^{-2}$, respectively[50–52].

We also examine the effect of interaction on band mixing with realistic experimental parameters. The scale of the Coulomb interaction is given by $\frac{e^2}{4\pi\epsilon R}$. The ratio of the interaction scale to the flat-band gap can be calculated as $\frac{m_e e^2 R}{4\pi\epsilon(l+1)\hbar^2}$. It is well known that for $Q > 0$, $R = \sqrt{Q} l_B$, where $l_B = \sqrt{\frac{\hbar}{eB}}$ is the magnetic length. Consequently, Landau level mixing can be suppressed by either increasing the magnetic field or decreasing Q. However, in the case of $Q = 0$ we no longer has a magnetic length, so the radius of the sphere is the only length scale. For Coulomb interaction at zero field not to mix different flat bands, it needs to be smaller than the gap ΔE_k^l of the flat band and greater than $k_B T$, so the radius R of the sphere must satisfy two conditions. The first condition is $R \ll \frac{4\pi\epsilon(l+1)\hbar^2}{m_e e^2}$. Here we take

$$R_1 = \frac{4\pi\epsilon(l+1)\hbar^2}{10 m_e e^2}, \tag{19}$$

which ensures $R \le R_1$. The second condition is $R < \frac{e^2}{4\pi\epsilon k_B T}$, and we take

$$R_2 = \frac{e^2}{8\pi\epsilon k_B T}, \tag{20}$$

ensuring $R \le R_2$. We can use the first condition in Eq. (19) and Eq. (17) to derive the minimum value of electron density

$$\rho_{\min} = \frac{25 m_e^2 e^4 l^2}{8\pi^3 \epsilon^2 (l+1)^2 \hbar^4}, \tag{21}$$

For large values of l, the ratio $\frac{l^2}{(l+1)^2}$ approaches 1. This implies that to reduce the required electron density, materials with a larger permittivity and a smaller effective mass are needed, such as InSb with $\epsilon = 17\epsilon_0$ (ϵ_0 is the vacuum permittivity)[53], and $\rho_{\min} \approx 3.8 \times 10^{11}\ \text{cm}^{-2}$. Using this density and the second condition in Eq. (20), we can calculate the required radius of the sphere at a temperature of 1 mK, which is approximately less than 0.49 mm.

Overall, at zero magnetic field, a flat band can be realized on a conducting sphere with a radius on the order of 10 to 100 microns, featuring an energy gap ranging from approximately 0.07 to 0.7 K and a degeneracy of 10^3 to 10^4 states. These parameters can be further optimized with improved material properties, such as a lower effective electron mass, higher electron density, and larger permittivity. In comparison, under a strong magnetic field of 10 tesla, a sample of approximately 1 micron by 1 micron hosts a similar order of magnitude for the number of states in each Landau level flat band, also around 10^3 states. InSb emerges as a promising candidate, capable of supporting flat bands with a degeneracy of up to 10^5 at 1 mK, corresponding to a maximum sphere radius of approximately 0.78 mm. The fabrication of micron-scale spherical substrates is well-established across various experimental fields[54,55], making this setup feasible. For higher temperatures or larger spheres, increasing the electron density of the material becomes essential, which is equally important for realizing flat bands dominated by interactions without significant band mixing effects. It is noteworthy that the system considered here fundamentally differs from the conventional flat bands realized in quantum materials in the thermodynamic limit, where the degeneracy of the flat band approaches infinity. In our study, we focus on a finite spherical system that, nevertheless, can achieve a high degeneracy of orbitals at the same energy (mimicking the flat bands) with a large gap from the rest of the spectrum, potentially with experimentally accessible parameters. Furthermore, in conventional flat band systems, the large degeneracy in the thermodynamic limit comes with a finite band gap, while in our case the gap also increases with the degeneracy, a useful property from an experimental point of view.

Future work could explore how the generation of Bell pairs on spherical systems can be experimentally realized with conducting materials with high

electron density. In the Results section titled Rotational symmetry in flat bands, we considered a highly tuned distribution of delta potentials, highlighting the potential impact of disorder on the system. For orbitals with large angular momentum, the energy gap between adjacent orbitals is significantly large ($\Delta E_k^l = \frac{(l+1)\hbar^2}{m_e R^2}$), which strongly suppresses the mixing of different flat bands due to disorder. While the effects of disorder in Landau levels have been extensively studied[29,34], the role of disorder in the $Q = 0$ flat band on the surface of the sphere remains an open question and will be the subject of future exploration. Furthermore, in the absence of a magnetic field, the impact of electron spin in this system and the novel phenomena it may induce will also be investigated in detail in future studies.

Data availability

All numerical data generated in this study are provided in the Supplementary Information and the Supplementary Data. Source Data are available with this paper.

Code availability

The code developed to analyze the results is available from the corresponding author upon reasonable request.

Received: 10 January 2025; Accepted: 25 June 2025;
Published online: 28 July 2025

References

1. Roy, R. & Sondhi, S. Fractional quantum Hall effect without Landau levels. *Physics* **4** https://doi.org/10.1103/Physics.4.46 (2011).
2. Parameswaran, S. A., Roy, R. & Sondhi, S. L. Fractional quantum Hall physics in topological flat bands. *Comptes Rendus Phys.* **14**, 816 (2013).
3. Bergholtz, E. J. & Liu, Z. Topological flat band models and fractional Chern insulators. *Int. J. Mod. Phys. B* **27**, 1330017 (2013).
4. Ramires, A. & Lado, J. L. Emulating heavy fermions in twisted trilayer graphene. *Phys. Rev. Lett.* **127**, 026401 (2021).
5. Tran, M.-T. & Nguyen, T. T. Molecular Kondo effect in flat-band lattices. *Phys. Rev. B* **97**, 155125 (2018).
6. Dong, J.-J. & Yang, Y.-f. Development of long-range phase coherence on the Kondo lattice. *Phys. Rev. B* **106**, L161114 (2022).
7. Iglovikov, V. I. et al. Superconducting transitions in flat-band systems. *Phys. Rev. B* **90**, 094506 (2014).
8. Cao, Y. et al. Unconventional superconductivity in magic-angle graphene superlattices. *Nature* **556**, 43 (2018).
9. Kopnin, N. B., Heikkilä, T. T. & Volovik, G. E. High-temperature surface superconductivity in topological flat-band systems. *Phys. Rev. B* **83**, 220503 (2011).
10. Yankowitz, M. et al. Tuning superconductivity in twisted bilayer graphene. *Science* **363**, 1059 (2019).
11. Mott, N. F. Metal-insulator transition. *Rev. Mod. Phys.* **40**, 677 (1968).
12. Hu, D., Dong, J.-J., Huang, L., Wang, L. & Yang, Y.-f. Effective classical correspondence of the Mott transition. *Phys. Rev. B* **101**, 075111 (2020).
13. Laughlin, R. B. Anomalous quantum Hall effect: An incompressible quantum fluid with fractionally charged excitations. *Phys. Rev. Lett.* **50**, 1395 (1983).
14. Yang, Y. & Hu, Z.-X. Monte carlo simulation of the topological quantities in fractional quantum Hall systems. *Phys. Rev. B* **107**, 115162 (2023).
15. Haldane, F. D. M. Fractional quantization of the Hall effect: A hierarchy of incompressible quantum fluid states. *Phys. Rev. Lett.* **51**, 605 (1983).
16. Haldane, F. D. M. Many-particle translational symmetries of two-dimensional electrons at rational Landau-Level filling. *Phys. Rev. Lett.* **55**, 2095 (1985).
17. Ojha, P. C. & Berry, R. S. Angular correlation of two electrons on a sphere. *Phys. Rev. A* **36**, 1575 (1987).
18. Loos, P.-Fmc & Gill, P. M. W. Ground state of two electrons on a sphere. *Phys. Rev. A* **79**, 062517 (2009).
19. Seidl, M. Adiabatic connection in density-functional theory: Two electrons on the surface of a sphere. *Phys. Rev. A* **75**, 062506 (2007).
20. Ezra, G. S. & Berry, R. S. Correlation of two particles on a sphere. *Phys. Rev. A* **25**, 1513 (1982).
21. Watanabe, S. & Lin, C. D. Classification scheme of triply excited states from a molecular viewpoint. *Phys. Rev. A* **36**, 511 (1987).
22. Thompson, D. C. & Alavi, A. Two interacting electrons in a spherical box: An exact diagonalization study. *Phys. Rev. B* **66**, 235118 (2002).
23. Thompson, D. C. & Alavi, A. A comparison of Hartree-Fock and exact diagonalization solutions for a model two-electron system. *J. Chem. Phys.* **122**, 124107 (2005).
24. Alavi, A. Two interacting electrons in a box: An exact diagonalization study. *CHEM. PHYS. - CHEM PHYS* **113**, 7735 (2000).
25. Yang, L. & Yao, Z. Two and three electrons on a sphere: A generalized Thomson problem. *Phys. Rev. B* **97**, 235431 (2018).
26. Wu, T. T. & Yang, C. N. Dirac monopole without strings: Monopole harmonics. *Nucl. Phys. B* **107**, 365 (1976).
27. Wu, T. T. & Yang, C. N. Some properties of monopole harmonics. *Phys. Rev. D.* **16**, 1018 (1977).
28. Edmonds, A. R., https://doi.org/10.1515/9781400884186. *Angular Momentum in Quantum Mechanics* (Princeton University Press, Princeton, 1957)
29. Roy, N., Peng, B. & Yang, B. Superlattice-induced electron percolation within a single Landau level. *Phys. Rev. B* **110**, 195116 (2024).
30. Rakhmanov, E., Saff, E. B. & Zhou, Y. M. Minimal discrete energy on the sphere. *Math. Res. Lett.* **1**, 647 (1994).
31. Saff, E. B. & Kuijlaars, A. B. J. Distributing many points on a sphere. *Math. Intell.* **19**, 5 (1997).
32. Williamson, D. The evolution of dynamical cores for global atmospheric models. *J. R. Met. Soc. Jpn.* **85B**, 241 (2007).
33. González, Á. Measurement of areas on a sphere using Fibonacci and latitude–longitude lattices. *Math. Geosci.* **42**, 49 (2010).
34. Peng, B., Roy, N., Ji, G., and Yang, B. Robust translational invariance in topological bands against lattice potentials and disorders https://arxiv.org/abs/2411.16862 (2024).
35. Trugman, S. A. & Kivelson, S. Exact results for the fractional quantum Hall effect with general interactions. *Phys. Rev. B* **31**, 5280 (1985).
36. Wang, J., Cano, J., Millis, A. J., Liu, Z. & Yang, B. Exact Landau level description of geometry and interaction in a flatband. *Phys. Rev. Lett.* **127**, 246403 (2021).
37. Sodemann, I. & MacDonald, A. H. Landau level mixing and the fractional quantum Hall effect. *Phys. Rev. B* **87**, 245425 (2013).
38. Rezayi, E. H. Landau level mixing and the ground state of the $\nu = 5/2$ quantum Hall effect. *Phys. Rev. Lett.* **119**, 026801 (2017).
39. Zhang, Y., Wójs, A. & Jain, J. K. Landau-level mixing and particle-hole symmetry breaking for spin transitions in the fractional quantum Hall effect. *Phys. Rev. Lett.* **117**, 116803 (2016).
40. Wójs, A. & Quinn, J. J. Landau level mixing in the $\nu = 5/2$ fractional quantum Hall state. *Phys. Rev. B* **74**, 235319 (2006).
41. Simon, S. H. & Rezayi, E. H. Landau level mixing in the perturbative limit. *Phys. Rev. B* **87**, 155426 (2013).
42. Rezayi, E. H. & Haldane, F. D. M. Lowest-order Landau-level mixing corrections for $4 \geq \nu > 2$ quantum Hall effect. *Phys. Rev. B* **42**, 4532 (1990).
43. Yang, B. Three-body interactions in generic fractional quantum Hall systems and impact of Galilean invariance breaking. *Phys. Rev. B* **98**, 201101 (2018).
44. Padmanabhan, M., Gokmen, T. & Shayegan, M. Composite fermion valley polarization energies: Evidence for particle-hole asymmetry. *Phys. Rev. B* **81**, 113301 (2010).

45. Maryenko, D. et al. Temperature-dependent magnetotransport around $\nu = 1/2$ in ZnO heterostructures. *Phys. Rev. Lett.* **108**, 186803 (2012).
46. Morf, R. H. Transition from quantum Hall to compressible states in the second Landau level: New light on the $\nu = 5/2$ enigma. *Phys. Rev. Lett.* **80**, 1505 (1998).
47. Rezayi, E. H. & Simon, S. H. Breaking of particle-hole symmetry by Landau level mixing in the $\nu = 5/2$ quantized Hall state. *Phys. Rev. Lett.* **106**, 116801 (2011).
48. Simon, S. H., Rezayi, E. H. & Cooper, N. R. Pseudopotentials for multiparticle interactions in the quantum Hall regime. *Phys. Rev. B* **75**, 195306 (2007).
49. Qi, Y. et al. Recent progress in strain engineering on Van der Waals 2d materials: Tunable electrical, electrochemical, magnetic, and optical properties. *Adv. Mater.* **35**, 2205714 (2023).
50. Wang, C. et al. Fractional quantum Hall state at filling factor $\nu = 1/4$ in ultra-high-quality GaAs two-dimensional hole systems. *Phys. Rev. Lett.* **131**, 266502 (2023).
51. Lei, Z. et al. High-quality two-dimensional electron gas in undoped InSb quantum wells. *Phys. Rev. Res.* **4**, 013039 (2022).
52. Ghosh, R. K., Brahma, M. & Mahapatra, S. Germanane: A low effective mass and high bandgap 2-d channel material for future FETs. *IEEE Trans. Electron Devices* **61**, 2309 (2014).
53. Rustagi, K. C. Effect of carrier scattering on nonlinear optical susceptibility due to mobile carriers in InSb, InAs, and GaAs. *Phys. Rev. B* **2**, 4053 (1970).
54. Okamoto, S. et al. Fabrication of single-crystalline microspheres with high sphericity from anisotropic materials. *Sci. Rep.* **4**, 5186 (2014).
55. Wilcox, D. L. & Berg, M. Microsphere fabrication and applications: an overview. *MRS Proc.* **372**, 3 (1994).

Acknowledgements

This work was supported by National Natural Science Foundation of China Grant No. 12474140 and 12347101, Chongqing Talents: Exceptional Young Talents Project No. cstc2021ycjh-bgzxm0147 and the Fundamental Research Funds for the Central Universities Grant No. 2024CDJXY022. C.-X. Jiang acknowledges the support of the China Scholarship Council Grant No. 202406050101. B. Yang is supported by the NTU grant for the National Research Foundation, Singapore under the NRF fellowship award (NRF-NRFF12-2020-005), Singapore Ministry of Education (MOE) Academic Research Fund Tier 3 Grant (No. MOE-MOET32023-0003) "Quantum Geometric Advantage", and Singapore Ministry of Education (MOE) Academic Research Fund Tier 2 Grant (No. MOE-T2EP50124-0017).

Author contributions

C.J. performed the theoretical and numerical calculations. Z.H. and B.Y. supervised the work.

Competing interests

The authors declare no competing interests.

Additional information

Supplementary information The online version contains supplementary material available at https://doi.org/10.1038/s42005-025-02208-9.

Correspondence and requests for materials should be addressed to Zi-Xiang Hu or Bo Yang.

Peer review information *Communications Physics* thanks Hayk Sarkisyan, Vasil Saroka and the other, anonymous, reviewer(s) for their contribution to the peer review of this work. A peer review file is available.

Reprints and permissions information is available at http://www.nature.com/reprints

Publisher's note Springer Nature remains neutral with regard to jurisdictional claims in published maps and institutional affiliations.

Open Access This article is licensed under a Creative Commons Attribution-NonCommercial-NoDerivatives 4.0 International License, which permits any non-commercial use, sharing, distribution and reproduction in any medium or format, as long as you give appropriate credit to the original author(s) and the source, provide a link to the Creative Commons licence, and indicate if you modified the licensed material. You do not have permission under this licence to share adapted material derived from this article or parts of it. The images or other third party material in this article are included in the article's Creative Commons licence, unless indicated otherwise in a credit line to the material. If material is not included in the article's Creative Commons licence and your intended use is not permitted by statutory regulation or exceeds the permitted use, you will need to obtain permission directly from the copyright holder. To view a copy of this licence, visit http://creativecommons.org/licenses/by-nc-nd/4.0/.

© The Author(s) 2025